metals

MDPI

Article

Effect of Solution Heat Treatment on the Porosity Growth of Nickel-Based P/M Superalloys

Hengyong Bu *, Lu Chen and Yonghua Duan

Faculty of Materials Science and Engineering, Kunming University of Science and Technology, Kunming 650093, China

* Correspondence: buhengyong@kust.edu.cn

Abstract: Thermal-induced porosity (TIP) is one of the major defects in powder metallurgy (P/M) superalloys, and it seriously affects the performance of P/M superalloys. The effects of solution heat treatment on the growth of the TIP of the nickel-based P/M superalloy FGH97 were investigated. A series of solution heat treatment tests were carried out at holding temperatures ranging from 1150 to 1200 °C, with holding times ranging from 0.5 to 8 h. The results showed that the holding time, temperature, and the initial volume of porosity are the primary factors influencing porosity growth, and the volume fraction of TIPs increases by increasing the temperature or extending the holding time. The porosity growth models were constructed based on the porosity statistics combined with a nonlinear fitting method. To evaluate the accuracy of the proposed models, the correlation coefficient (R) and average absolute relative error ($AARE$) were calculated between the predicted and experimental values. The unbiased $AARE$ values were 2.06% and 3.99% for the average value of TIP and the worst value of TIP, respectively, which imply that the proposed porosity growth models have greater accuracy and can be used to illustrate TIP behavior in solution heat treatment.

Keywords: solution heat treatment; thermal-induced porosity; TIP growth model; nickel-based P/M superalloy

Citation: Bu, H.; Chen, L.; Duan, Y. Effect of Solution Heat Treatment on the Porosity Growth of Nickel-Based P/M Superalloys. *Metals* **2022**, *12*, 1973. https://doi.org/10.3390/met12111973

Academic Editors: Satoru Kobayashi and Mikael Perrut

Received: 11 October 2022
Accepted: 16 November 2022
Published: 18 November 2022

1. Introduction

Superalloys are widely used for gas turbines, aircraft engines, chemical process industries, and other high-temperature environment components requiring heat and/or oxidation resistance due to their superior performances at elevated temperatures [1–3]. With the development of modern aerospace industries, the engine's thrust-to-weight ratio is expected to reach a high level [4], which means that turbine disks will face much higher temperatures and pressures. To respond to this challenge and improve superalloy performance, the traditional casting/forging methods like to add a large number of alloy elements into the superalloy, which could result in significant segregation, inhomogeneous microstructure, and unstable precipitates [4,5]. The above defects within the superalloy will be more serious when the dimensions of the parts exceed a critical value [5]. In the 1960s, powder metallurgy was invented and considered the ideal routine for manufacturing superalloy components, which can eliminate segregation and significantly improve mechanical performance [2,4–6].

Compared to casting/forging nickel superalloys, nickel-based P/M superalloys present so many advantages, such as fine particle size, homogeneous chemical composition, uniform microstructure, high yield strength, high-temperature stability, low fatigue crack growth rate, and relatively low expense [5,7,8]. As a result, nickel-based P/M superalloys are becoming the essential material for manufacturing aircraft engine components, including turbine disks, which are among the most critical components in the aeroengine [7]. In pursuit of higher thermal efficiency and lower emissions, innovative techniques and alloys with additional elements have been invented and applied, which raise the working

temperature and enhance the creep life to a new level. There are already three generations of nickel-based P/M superalloys in China. FGH95 and FGH97 belong to the first generation, with an operation temperature restricted to 650 °C. The second-generation FGH96 alloy has a superior damage tolerance and can withstand higher working temperatures. Naturally, the third generation of the nickel-based P/M superalloy has significantly higher operating temperatures and thermal stability than the first- and second-generation superalloys [9].

Generally, defects cause deterioration in the performances of metallic materials. Inclusions, prior particle boundary (PPB), and thermal-induced porosity (TIP) are three primary defects in P/M superalloys [10]. It is believed that there are three reasons that can cause the TIP [10–14], and the first one is entrapped insoluble gas, likely due to the hollow powder that forms during argon atomization, which expands during heat treatments after hot isostatic pressing (HIP), eventually causing the formation of discontinuous porosity in the components. The second reason is that insoluble gases absorbed into the surface of the powder are not completely removed before the HIP process. Finally, there may be a leakage in the container, and the inert gas is introduced into the powders during the HIP process.

The effects of TIP on the mechanical properties of nickel-based P/M superalloys have been extensively studied and has shown that TIP has a significant detrimental effect on alloy performance. With the increase in TIP, the yield strength, ultimate tensile strength, impact toughness, rupture life, fatigue limit, and elongation of the superalloys decrease accordingly [13–15]. Additionally, when the volume fraction of TIP within the component reaches a critical level, it not only makes the component prone to warping but also easily becomes the source of cracks during heat treatment [13]. Zhang et al. [13] found that the impact energy of the FGH95 alloy was reduced by 58.18% as the porosity increased from 0.072% to 1.744%. It was also found that the tension and stress rupture strengths of porous materials were reduced by less than 7% at high temperatures, and the tensile ductility was reduced by 40% for Astroloy alloy; its creep–fatigue life was approximately 30% lower for the porous materials than for full-density materials [15]. Wang et al. [16] investigated the formation of TIPs in the FGH95 and Rene 95 P/M superalloys by measuring densities before and after solution heat treatments and found that TIP increased with increasing temperature and time. It illustrated that the temperature and time of the solution heat treatments are two major factors that affect the TIP in nickel-based P/M superalloys. However, neither the quantitative model for predicting TIP nor the relationship between the solution heat treatment parameters and TIP were provided. Several models have been proposed to simulate porosity growth in the past few decades, but most of them focused on aluminum and steel alloys [17,18]. Lee et al. [19] simulated the pore growth in the Al–Cu alloy caused by hydrogen diffusion through a 2D continuum diffusion model and a stochastic pore nucleation model. Carlson et al. [20] proposed a volume-average model for the finite rate diffusion of hydrogen in aluminum alloys. Monastyrskiy [21] developed a modeling tool to model the formation of shrinkage porosity in a GS 32 Ni-based superalloy with low gas content based on liquid metal deformation due to solidification. Bokstein et al. [22] constructed an analytical model for the pore formation during the homogenization process of nickel-based single-crystal superalloys based on the unbalanced cross-diffusion of the alloy elements. However, research on the porosity model for nickel-based superalloys was seldom mentioned [23].

In this paper, the effects of the solution heat treatment parameters on the porosity growth of the nickel-based P/M FGH97 superalloy were investigated, and a series of solution heat treatment tests were carried out at temperatures ranging from 1150 to 1200 °C, with holding times ranging from 0.5 to 8 h. With the assistance of microstructure observation, TIP growth models were established to describe the relationships among the temperature, time, and the initial volume fraction of TIPs. The predictive accuracy of the models was evaluated by calculating the correlation coefficient (R) and the average absolute relative error ($AARE$).

2. Materials and Experimental Procedures

The nickel-based P/M FGH97 superalloy used in this study was provided by the Shenzhen Wedge Central South Research Institute Company. The superalloy was prepared using argon-atomized powder with a median diameter of about 50 μm and then consolidated into a disk with a diameter of 145 mm and a height of 100 mm by hot isostatic pressing. The main parameters, including temperature, pressure, and holding time, used in the HIP process were set at 1200 °C, 120 MPa, and 2 h, respectively. The chemical composition of the FGH97 superalloy is given in Table 1, which is similar to the Russian-made EP741NP nickel-based P/M superalloy. Due to the different degree of leakage of the containers, turbine disks with three different initial volumes of porosity were selected as raw materials, and referred to as Ni1#, Ni2#, and Ni3#, respectively. Solution heat treatments were carried out using a DIL 805A dilatometer machine (TA Instruments, Hüllhorst, Germany), and cylindrical specimens with a diameter of 4 mm and length of 10 mm were used. All the specimens were cut from Ni1#, Ni2#, and Ni3# using wire electrolytic discharge. A type S (Pt-Pt/Rh10%) thermocouple was spot-welded in the center of the specimen surface, which was used for the closed-loop temperature control of the specimen. Cylindrical specimens in solution heat treatment tests were heated using induction and cooled using helium gas. The helium gas at room temperature was ejected from the holes on the inner surface of the induction coil and hit the specimen surface, cooling the specimen. Consequently, precise control of the specimen temperature was achieved by dynamically adjusting the heating power and gas flow rate.

Table 1. Chemical composition of the studied P/M FGH97 superalloy (wt. %).

Composition	Co	Cr	Al	Ti	W	Mo	Hf	Nb	Ni
wt. %	16.11	8.92	5.19	1.85	5.57	3.81	0.19	2.49	Bal.

The solution heat treatment procedure is shown in Figure 1. All specimens were heated from room temperature to 1150, 1175, and 1200 °C with a heating rate of 2 K/s, held for 0.5, 2, 4, and 8 h, and then quenched to room temperature with a cooling rate of 40 K/s. It has been reported that the solvus temperature of the γ′ phase is about 1190 °C [24], which implies that the solution heat treatment with the temperatures of 1150 and 1175 °C belonged to the sub-solvus heat treatment, and the 1200 °C belonged to the super-solvus heat treatment. The heat-treated samples were sectioned, grinded, polished, and etched using the standard metallographic method. It should be noted that the samples were etched with a chemical etchant of 5 g of $CuCl_2$ + 100 mL of HCl + 100 mL of ethanol. TESCAN VEGA3 scanning electron microscopy (SEM) (Tescan, Brno-Kohoutovice, Czech Republic), with secondary electron (SE) and back-scattering electron (BSE) mode, and optical microscopy (OM) were used for microstructure observation. OM images with ×150 magnifications were collected to evaluate the volume fraction of the TIP using an automatic image software. The relationships among the temperature, time, and the initial volume fraction of TIP were investigated using stereological metallography and image analysis according to the standard GB/T 15749-2008 [25].

Two statistical methods were used in this study to estimate the volume fraction of TIP, and the first one is that the average value of the TIP was considered the reference value, called the average value of TIP later in the discussion. The other used at least three random OM images (at least 100 pores in total), and the maximum TIP value of the images was selected as the reference value and named the worst value of TIP.

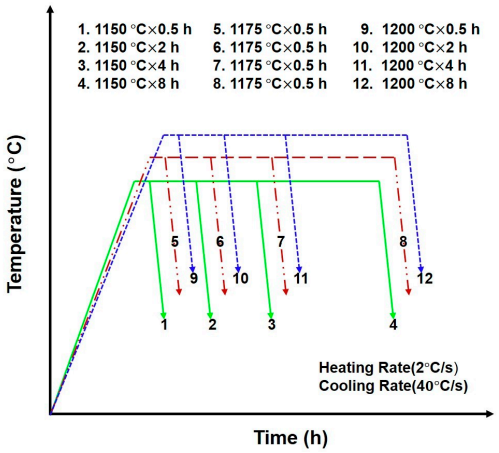

Figure 1. Schematic of solution heat treatment tests for the P/M FGH97 superalloy.

3. Results and Discussion

3.1. TIP of the as-HIPed FGH97 Superalloys

The OM images of the as-HIPed FGH97 superalloys are shown in Figure 2. It can be seen that there were plenty of TIPs in the Ni1# alloy, and they were distributed nonuniformly; the number of TIPs in the Ni2# alloy was significantly lower, and its distribution was relatively uneven. The Ni3# alloy was the only qualified superalloy; the TIPs could seldom be found, and it could be used in high-temperature components with further processing. It should be mentioned that the as-HIPed superalloys had been subjected to hot isostatic pressing, during which the powders consolidated by using high-pressure argon under high temperatures. HIP concerns many sophisticated phenomena, including deformation, creep, diffusion, precipitates evolution, and plastic deformation induced by dislocation slip, which are considered key issues for TIP healing [26]. However, a certain number of TIPs remained in the superalloys after HIP, which implied that the TIP was not healed during the HIP process.

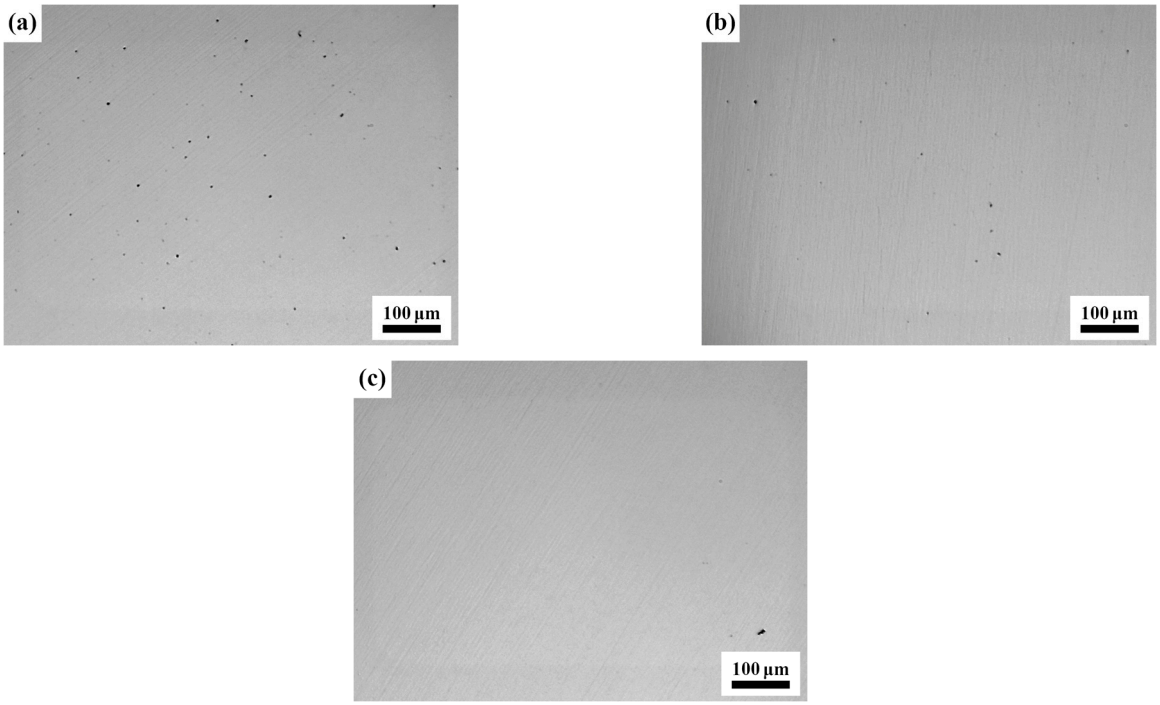

Figure 2. OM images of the as-HIPed P/M FGH97 superalloys, (**a**) Ni1#, (**b**) Ni2#, and (**c**) Ni3#.

To eliminate the inclusions and improve the low-cycle fatigue performance, the powder used for the FGH97 superalloy was prepared using argon atomization (AA) rather than plasma-rotating electrode atomization (PREP). However, it has been reported that the powder that used the former method had more defects than the latter, such as high oxygen content and more hollow powder [27]. Additionally, stainless steel powder containers of Ni1# and Ni2 # were not vacuumed to a standard level, and air leakage may occur during the HIP processing; that was why the TIP values of the Ni1# and Ni2# were higher than that of Ni3#. Despite the high temperatures and pressures that were used in the HIP process, argon gas was incapable of diffusing out of the container or dissolving in the superalloy [28], and the argon gas swelled at elevated temperatures, causing internal stresses that prevented subsequent densification. Moreover, no deformation process was applied to the densified disks, and TIP still remained in the superalloys [29].

SEM images of the as-HIPed specimen (Ni3#) are shown in Figure 3; they were taken at the same position of the specimen's cross-section but with different modes, with left being SE mode and right being BSE mode. Almost nothing could be detected in the SE mode; the deeper gray scale region in the BSE mode was identified as the γ' phase. That means the SEM image with BSE mode was beneficial for observing the microstructure. The details of the evolution of the precipitate during the HIP process and subsequent solution heat treatment are not shown here. It is difficult to distinguish the γ' phase from the TIPs, as they have a similar grayscale, regardless of whether they are in SE or in BSE mode. Therefore, OM images were selected for TIP evaluation, not only because they have a greater view field than SEM images, but also because they are beneficial for statistical analysis.

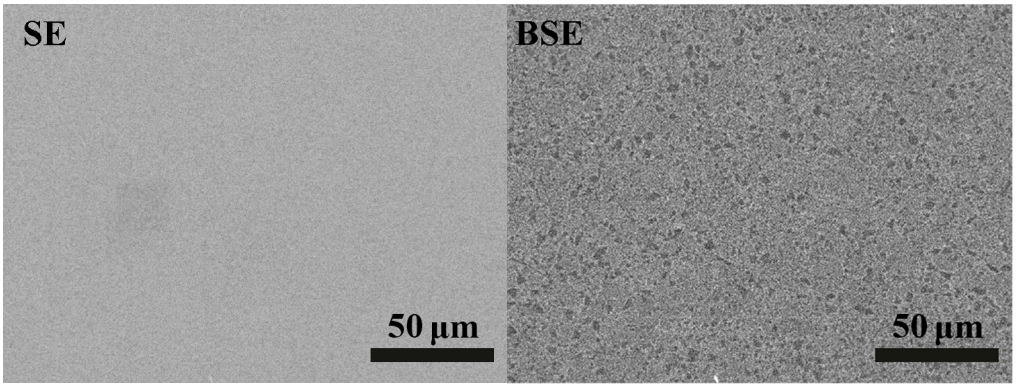

Figure 3. SEM morphology of the as-HIPed Ni3# specimen.

The volume fractions of the TIP based on OM images of Ni1#, Ni2#, and Ni3# superalloys were statistically analyzed, respectively. The TIP values of the as-HIPed FGH97 superalloys are presented in Figure 4. The result showed that there was a significant difference in the TIP volume fractions between the two measurement methods mentioned above, but they had the same trend. The Ni1# superalloy had the highest TIP value, followed by the Ni2#, and the Ni3# had the lowest value, which is consistent with the findings of the OM observation shown in Figure 2. It also demonstrated that the HIP conditions, such as vacuum level and compactness of the container, had remarkable impacts on the TIP values of the nickel-based superalloys.

3.2. TIP Evolution during Solution Heat Treatment

The OM images of the P/M FGH97 superalloys under different solution heat treatment conditions are presented in Figures 5–7, respectively. The holding temperatures were set at 1150, 1175, and 1200 °C, with holding times of 0.5, 2, 4, and 8 h. The volume fraction of the TIP increased with increasing holding temperature or holding time, and the size of the TIP became larger than the as-HIPed specimens. The shapes of the porosity also changed with the increase in holding time and temperature because high-temperature and long-term preservation promoted the diffusion of the elements and the accumulation of

the porosity; this can be seen in Figures 5l, 6i and 7l, which had much lower numbers of porosities than low-temperature or short-term solution heat treatment. Table 2 presents the size and shape factors of the TIP of the specimens before (as-HIPed) and after high-temperature solution heat treatment (Figures 5l, 6i and 7l). The average sizes of the TIPs of the as-HIPed specimens were 4.0, 3.5, and 3.4 μm of the Ni1#, Ni2#, and Ni3# superalloys, respectively. Apparently, the differences between these size values were not so different, considering that the same raw powder and HIP parameters were used; the initial volume fractions of the TIPs and their sizes may interact with each other. Moreover, the average sizes of the TIPs increased several times, and the shapes of the porosities became irregular after the solution heat treatment, which is consistent with the results obtained from the OM observation.

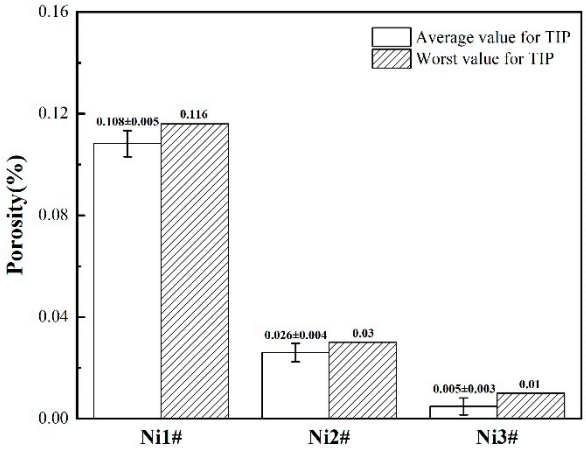

Figure 4. Initial TIP values of the as-HIPed P/M FGH97 superalloys.

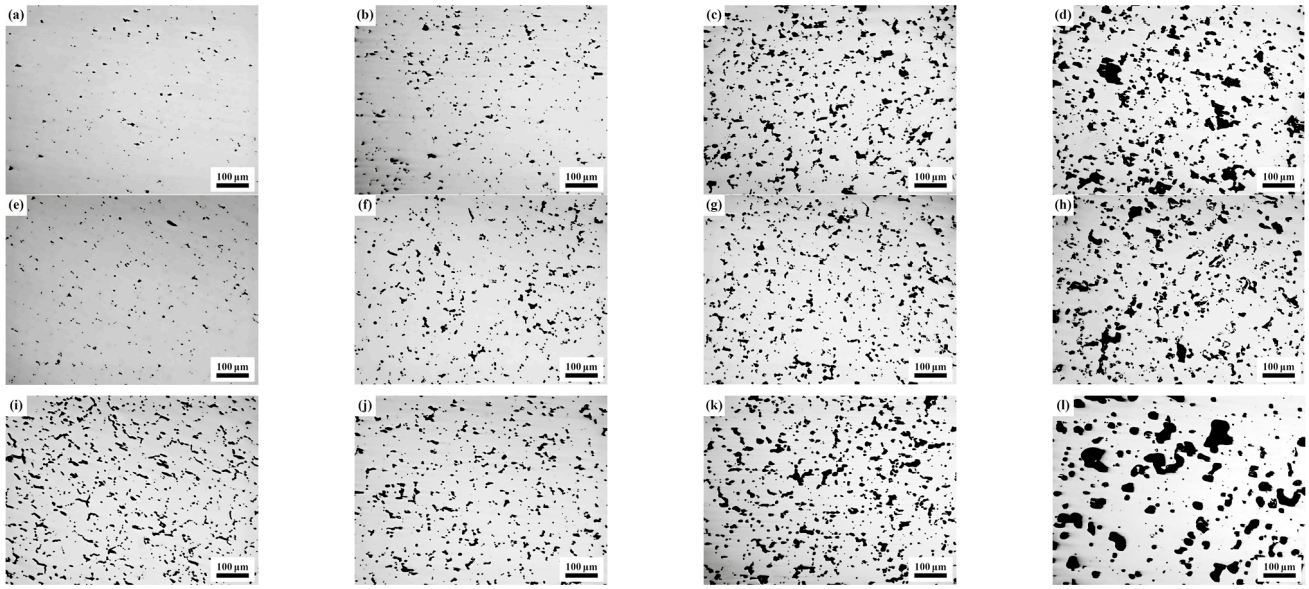

Figure 5. OM images of the Ni1# superalloy after solution heat treatment, (**a**) 1150 °C × 0.5 h, (**b**) 1150 °C × 2 h, (**c**) 1150 °C × 4 h, (**d**) 1150 °C × 8 h, (**e**) 1175 °C × 0.5 h, (**f**) 1175 °C × 2 h, (**g**) 1175 °C × 4 h, (**h**) 1175 °C × 8 h, (**i**) 1200 °C × 0.5 h, (**j**) 1200 °C × 2 h, (**k**) 1200 °C × 4 h, and (**l**) 1200 °C × 8 h.

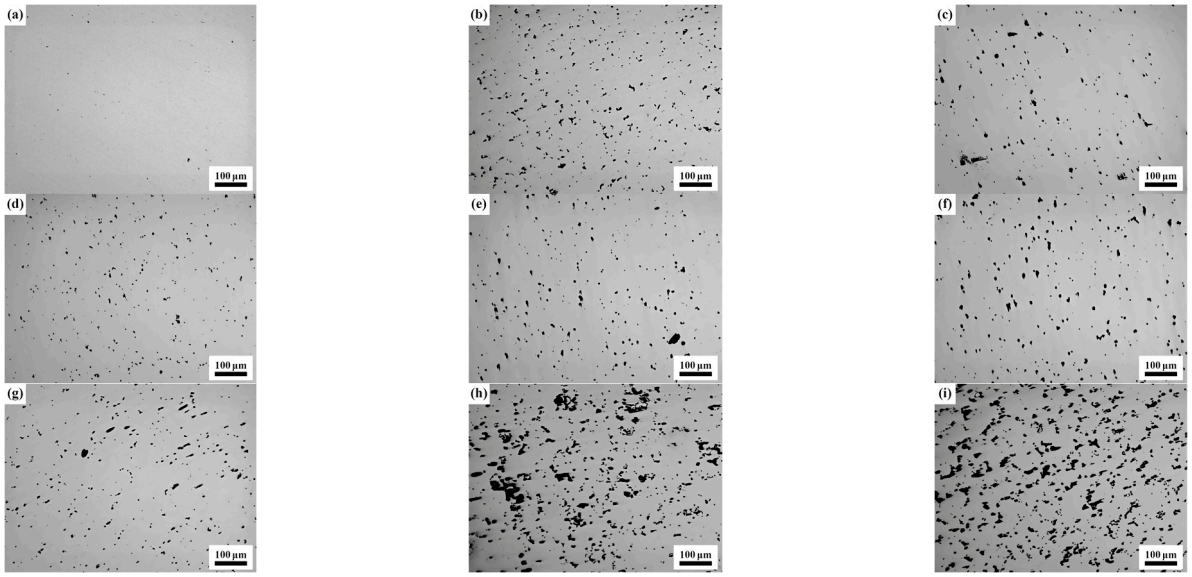

Figure 6. OM images of the Ni2# superalloy after solution heat treatment, (**a**) 1150 °C × 0.5 h, (**b**) 1150 °C × 2 h, (**c**) 1150 °C × 4 h, (**d**) 1175 °C × 0.5 h, (**e**) 1175 °C × 2 h, (**f**) 1175 °C × 4 h, (**g**) 1200 °C × 0.5 h, (**h**) 1200 °C × 2 h, and (**i**) 1200 °C × 4 h.

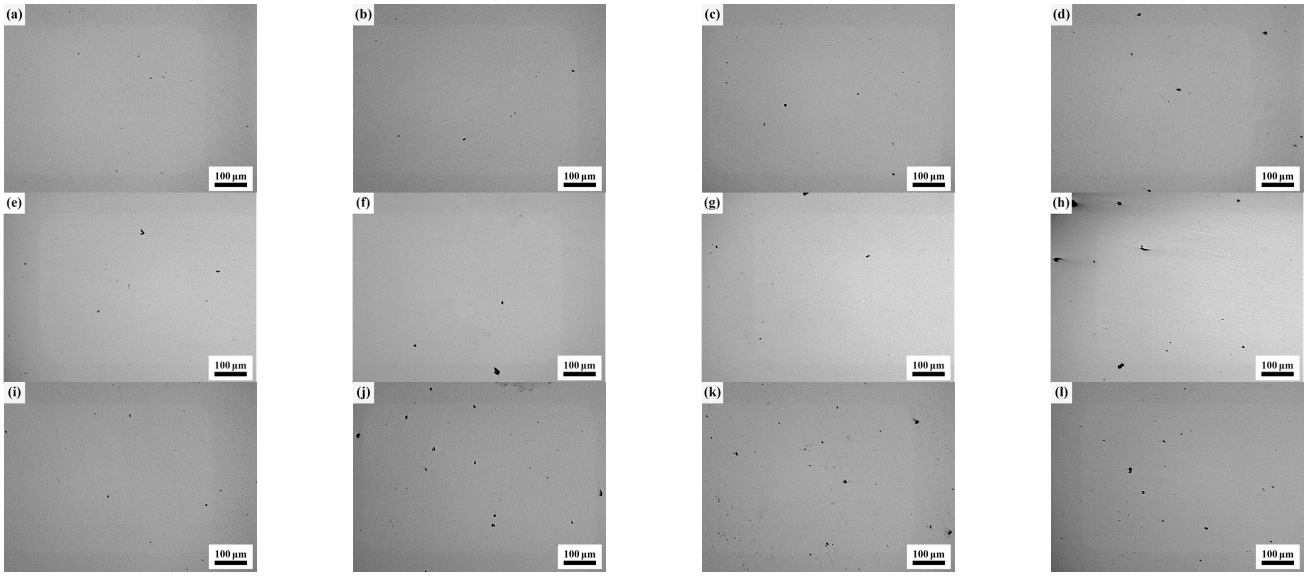

Figure 7. OM images of the Ni3# superalloy after solution heat treatment, (**a**) 1150 °C × 0.5 h, (**b**) 1150 °C × 2 h, (**c**) 1150 °C × 4 h, (**d**) 1150 °C × 8 h, (**e**) 1175 °C × 0.5 h, (**f**) 1175 °C × 2 h, (**g**) 1175 °C × 4 h, (**h**) 1175 °C × 8 h, (**i**) 1200 °C × 0.5 h, (**j**) 1200 °C × 2 h, (**k**) 1200 °C × 4 h, and (**l**) 1200 °C × 8 h.

Table 2. The sizes and shape factors of the TIPs of the as-HIPed specimens and the specimens after high-temperature solution heat treatment.

as-HIPed	Average Value (%)	Worst Value (%)	Size (μm)	Shape Factor	Solution Heat Treated (1200 °C)	Size (μm)	Shape Factor
Ni1#	0.108 ± 0.005	0.116	4.0	0.94	Ni1#—8 h	17.2	0.74
Ni2#	0.026 ± 0.004	0.03	3.5	0.90	Ni2#—4 h	7.0	0.78
Ni3#	0.005 ± 0.003	0.01	3.4	0.91	Ni3#—8 h	6.8	0.88

The specimens were deformed after the solution heat treatment, particularly for the specimen held at a higher temperature and for a longer term; the shape of the cylinder was transformed into a drum, which can be seen in Figure 8. Compared with the cylindrical as-HIPed specimen, the solution heat treatment caused a severe and irregular deformation and even lead to specimen explosion. All Ni2# specimens exploded when the holding time increased to 8 h, regardless of the holding temperature, because the pressure of the trapped gas inside the TIPs exceeded a critical value and may cause permanent dimensional changes [30].

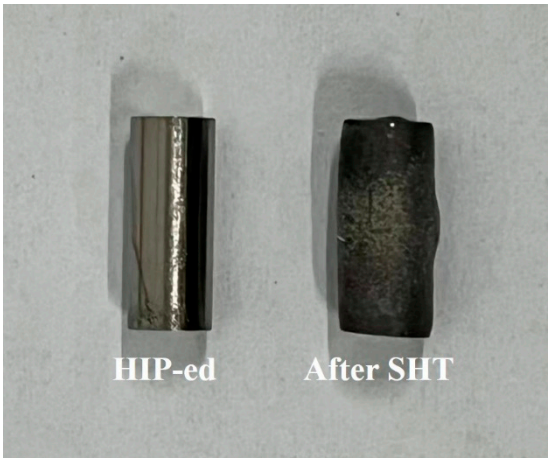

Figure 8. The shape of the Ni1# specimen before and after 1200 °C × 8 h solution heat treatment.

The growth mechanism of porosity is mainly diffusion, creeping, or both [31]. Previous studies have revealed that the time-dependent variation of porosities filled with argon gases attributed to the creep deformation of the surrounding materials [32]. With the increase in the holding temperature and the extension of the holding time, the argon pressure increased, and the deformation resistance decreased; the creep rate increased at the same time, leading to the TIPs growing more rapidly and increasing the TIP volume fraction more quickly [28].

As can be seen in the OM images, the TIPs were distributed nonuniformly across the metal matrix. In order to reveal the locations of the TIPs, specimens with different volumes of porosity were etched and are shown in Figure 9. The average grain sizes of Ni1#, Ni2#, and Ni3# after the same solution heat treatment (1175 °C × 2 h) were 23.7, 25.1, and 22.3 μm, respectively. It demonstrated that the differences in the grain sizes of the specimens were very small, even though they had different TIP values. The images of the Ni1# and Ni2# superalloys illustrated that TIPs are primarily located on the grain boundaries, known as inter-crystalline pores; similar results have been reported in Ref. [33]. Unlike the Ni3# specimen, almost no TIP could be detected because the volume fraction of the TIP of Ni3# was much lower than the other two specimens. TIP is most likely to form through gas diffusion at the intersection where the three grains meet. It also implies that the gas trapped in the specimens did not originate from the powder, but that the degassing treatment was incomplete, or some leakage occurred in the HIP process [14]. TIP growth is mainly dependent on the amount of trapped gas that forms during the hot isostatic pressing; the increase in gas pressure at elevated temperatures promotes the diffusion creep of the superalloys and results in an increase in porosity.

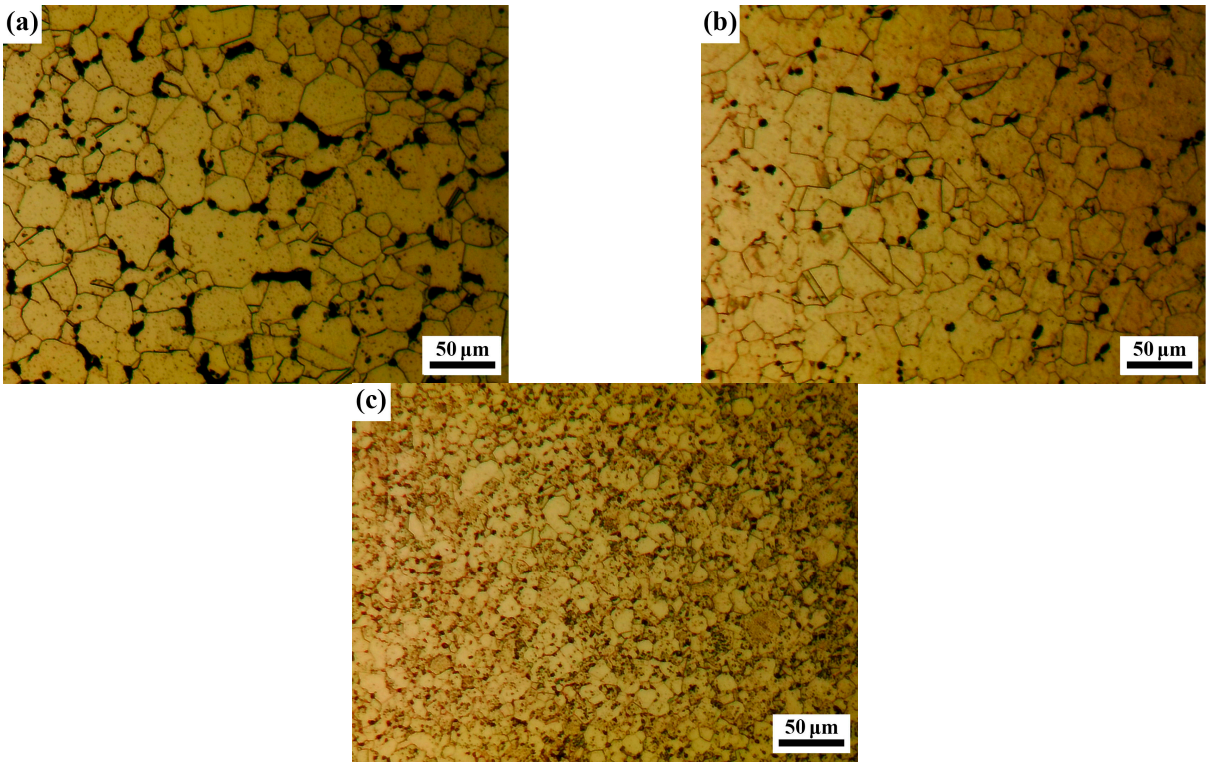

Figure 9. Microstructure of the FGH97 superalloy with different volumes of porosity after etching; (**a**) Ni1#, (**b**) Ni2#, and (**c**) Ni3#.

When the volume fraction of the initial porosity of the superalloy is large, microcracks are easily formed after solution heat treatment. With the increase in temperature and time, the TIP grows gradually and eventually reaches a critical size and connects to one another, leading to it forming an intergranular fracture path [31]. The cooling velocity of the specimens is 40 K/s after the solution heat treatment, it is large enough to produce stress concentration on the surface of the TIP, the expansion coefficient of the argon gas in the porosity is much higher than that of the superalloys, and the surrounding metallic matrix has subsequently deformed and the porosity increases. As a result, TIP can easily become the source of a crack and can be further expanded and connected to the surrounding TIPs, causing a macrocrack [13,34].

3.3. Description of TIP by Statistical Analysis

Figure 10a,b show the variations of the average/worst volume fractions of the TIP with the solution heat treatment parameters, respectively. It can be seen that with the increase in the initial volume fraction of porosity, holding temperature, and holding time, the volume fraction of the TIP increased after solution heat treatment. Although the average value of the TIP is generally accepted as the standard for assessing the quality and performance of nickel-based superalloys, the worst value of the TIP is probably the most valuable factor that can be used to estimate the creep properties and fatigue life. Similar results can be found in Figure 10b. the worst value of the TIP increases with the increasing of the holding temperature or holding time, particularly for superalloys Ni1# and Ni2#. However, Ni3# presents different TIP growth characteristics, and the worst value of the TIP fluctuated with temperature. There are two main reasons for data fluctuation: the first reason is that the size of the specimen section is limited, which means that the number of regions for statistical analysis is small; the other reason is that the TIP was distributed nonuniformly within the metallic matrix and observed in OM mode with 2D morphology.

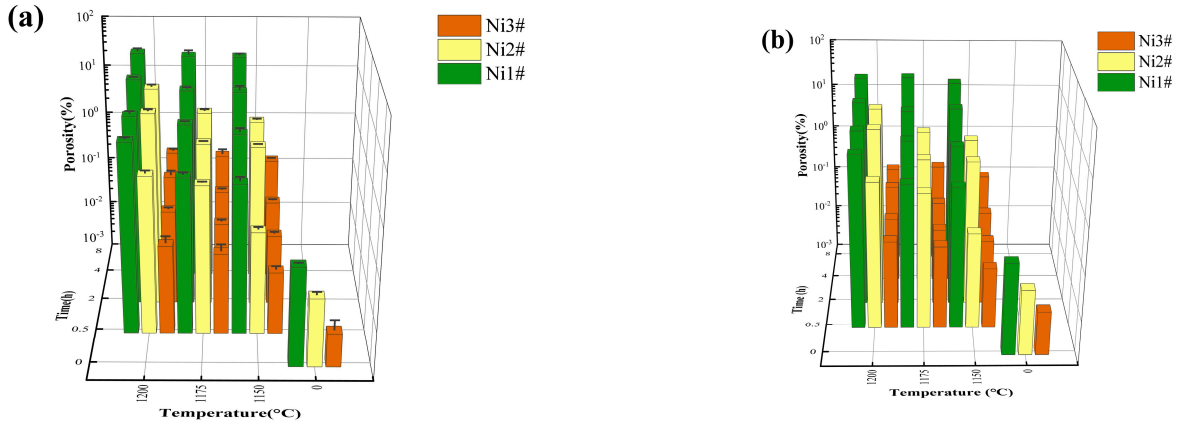

Figure 10. Evolution of the TIP as a function of holding temperature and holding time; (**a**) the average value of the TIP and (**b**) the worst value of the TIP.

It should be noted that the increase in the TIP volume fraction became large with increasing holding temperatures, which could mean that the effect of the holding temperature on TIP growth is much more significant than that of the holding time. Based on the results mentioned above, it can be concluded that the initial volume fraction of porosity, holding temperature, and holding time are the main factors that influence the porosity growth behavior. There was a positive correlation between the TIP value and the three main factors; similar findings were also reported in Ref. [16].

3.4. Porosity Growth Model

Sellars [35] found that the relationships among grain size, temperature, and time can be quantitatively represented as:

$$d^n = d_0^n + At\exp\left(-\frac{Q}{RT}\right) \quad (1)$$

where d is the average grain size, d_0 is the initial grain size, Q is the activation energy of grain growth (J/mol), A and n are the material constants, R is the gas constant (8.314 J/(mol·K)), T is the holding temperature, and t is the holding time.

Menasche [33] reported that gases that remain trapped in the powder-processed polycrystalline nickel-based superalloys will experience thermally activated diffusion during the subsequent heat treatment. The diffusion will be accelerated at the grain boundaries due to their high free volume. It can be seen from Equation (1) that the holding temperature and time are the main factors that affect the ability of the elements to diffuse, which has a greater influence on the evolution of grain size. The results of the solution heat treatment clearly show that TIP growth was influenced by temperature, time, and initial volume of porosity. Since the TIP growth is controlled by diffusion, creep, or both, the growth behavior follows a thermal activation process. A porosity growth model was developed to describe the TIP evolution of the FGH97 superalloy, which is given as follows:

$$P^n = P_0^n At\exp\left(-\frac{Q}{RT}\right) \quad (2)$$

where P is the volume fraction of the porosity after solution heat treatment, P_0 is the initial volume fraction of the porosity, and Q is the TIP growth activation energy (J/mol); the remaining parameters have the same meaning with Equation (1).

Based on the TIP statistical results, a nonlinear fitting method was used to obtain n, A, and Q in Equation (2), and their values are listed in Table 3. It should be noted that the calculation results of Q were close to the activation energy for the self-diffusion of Ni (about 260 kJ/mol) [36], which implies that TIP growth is dominated by diffusion.

Table 3. Calculation results of parameters in Equation (2).

Parameter	Average Value	Worst Value
A	8.09×10^{10}	2.88×10^{10}
Q	2.33×10^{5}	2.24×10^{5}
n	1.54	1.46

Substituting the parameters in Table 3 into Equation (2), the porosity growth models of FGH97 were solved as follows:

$$P^{1.54} = P_0^{1.54} \cdot 8.09 \times 10^{10} \cdot t \cdot \exp\left(-\frac{2.33 \times 10^5}{RT}\right) \quad (3)$$

(Average value of TIP)

$$P^{1.46} = P_0^{1.46} \cdot 2.88 \times 10^{10} \cdot t \cdot \exp\left(-\frac{2.24 \times 10^5}{RT}\right) \quad (4)$$

(Worst value of TIP)

The deviation of the calculational porosity from the experimental results was investigated quantitatively by using two parameters, the correlation coefficient (R) and average absolute relative error ($AARE$), as expressed in Equations (5) and (6).

$$R = \frac{\sum_{i=1}^{N}(E_i - \overline{E})(P_i - \overline{P})}{\sqrt{\sum_{i=1}^{N}(E_i - \overline{E})^2 \sum_{i=1}^{N}(P_i - \overline{P})^2}} \quad (5)$$

$$AARE = \frac{1}{N}\sum_{i=1}^{N}\left|\frac{P_i - E_i}{E_i}\right| \times 100\% \quad (6)$$

where E_i is the experimental value, P_i is the predicted value, $\overline{E}$ and $\overline{P}$ are the average of experimental and predictive values, and N is the number of data points. It should be noted that a higher R and lower $AARE$ value generally indicate higher predictive accuracy.

The correlation between the experimental and predicted porosity values which were calculated using Equations (3) and (4) are shown in Figure 11. The red line with a slope of 1 indicates the exact suitable position between the experimental and predicted values. There were a few data points that deviated from the red line but with a limited deviation range. The correlation coefficient (R) values were 0.94 for the average value of the TIP model and the worst value of the TIP model; all the values were close to 1. Moreover, the average absolute relative error ($AARE$) values were 2.06% and 3.99% of the two models, which means the proposed models are suitable to predict the average/worst values of the TIP after solution heat treatment.

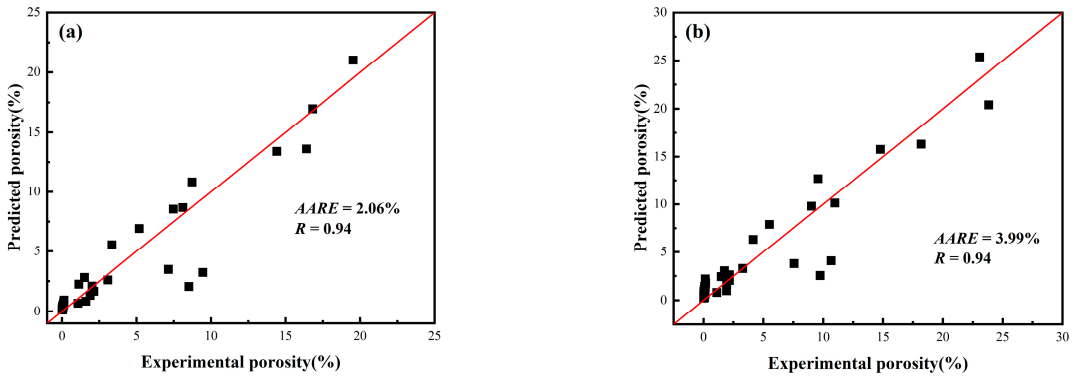

Figure 11. Correlation between the experimental and predicted values of porosity growth models; (**a**) the average value of the TIP and (**b**) the worst value of the TIP.

4. Conclusions

The porosity growth behavior during the solution heat treatment of the nickel-based P/M FGHT97 superalloy was investigated. Some conclusions could be drawn based on the above study.

1. The TIPs were distributed nonuniformly within the metallic matrix of the FGH97 superalloy, regardless of whether it was before or after solution heat treatment.
2. The initial volume fraction of porosity, holding temperature, and time are the primary factors that influence the porosity growth behavior, which has a positive correlation with the primary factors.
3. The TIP growth models were accurate in predicting the average/worst TIP values of the P/M FGH97 superalloys when the holding temperature ranged from 1150 to 1200 °C and holding time ranged from 0.5 to 8 h. The correlation coefficient value and the average absolute relative error value were 0.94 and 2.06% between the experimental and predictive average porosity values and 0.94 and 3.99% between the experimental and predictive worst porosity values.

Author Contributions: Conceptualization, H.B. and L.C.; methodology, H.B. and Y.D.; software, L.C. and Y.D.; validation, L.C.; formal analysis, L.C.; investigation, L.C. and H.B.; resources, H.B.; data curation, L.C.; writing—original draft preparation, H.B. and L.C.; writing—review and editing, H.B. and L.C.; visualization, H.B.; supervision, H.B.; project administration, H.B.; funding acquisition, H.B. All authors have read and agreed to the published version of the manuscript.

Funding: This research was funded by the Shenzhen Wedge Central South Research Institute Company, the Innovation Team Cultivation Project of Yunnan Providence, grant number 202005AE160016, and the Key Research and Development Program of Yunnan Providence, grant number 202103AA080017.

Data Availability Statement: Not applicable.

Acknowledgments: We thank the Shenzhen Wedge Central South Research Institute Company for providing funding, materials, and experimental assistance. The authors would also like to thank the Innovation Team Cultivation Project of Yunnan Providence (No. 202005AE160016) and the Key Research and Development Program of Yunnan Province (No. 202103AA080017) for their assistance.

Conflicts of Interest: The authors declare no conflict of interest.

References

1. Stoloff, N.S. *Metals Handbook*; ASM International: Novelty, OH, USA, 1990; Volume 1.
2. Guo, M.W.; Liu, C.R.; Zheng, X.P.; Liu, C.; Liu, S.L. Research status of powder metallurgy superalloy. *Hot Work. Technol.* **2017**, *46*, 11–13.
3. Donachie, M.J.; Donachie, S.J. *Superalloys a Technical Guide*; ASM International: Novelty, OH, USA, 2002.
4. Zou, J.W.; Wang, W.X. Development and application of P/M superalloy. *J. Aeron. Mater.* **2006**, *26*, 244–250.
5. Lei, J.F.; Zheng, Y.; Yu, J.; Lu, X.P.; Du, N. P/M Nickel-based superalloy. *Aerosp. Mater. Technol.* **2011**, *41*, 18–22.
6. Zhang, G.Q.; Zhang, Y.W.; Zheng, L.; Peng, Z.C. Research progress in powder metallurgy superalloys and manufacturing technologies for aero-engine application. *Acta Metall. Sin.* **2019**, *55*, 1133–1144.
7. Zhang, Y.W.; Liu, J.T. Development in powder metallurgy superalloy. *Mater. China.* **2013**, *32*, 1–11.
8. Shi, C.X.; Zhong, Z.Y. Development and innovation of superalloy in china. *Acta Metall. Sin.* **2010**, *46*, 1281–1288. [CrossRef]
9. Liu, X.L.; Tao, C.H.; Feng, Y.L.; Liang, J.; Wang, Y.B. *P/M Nickel-Based Superalloy Damage Behavior and Prediction*; Aviation Industry Press: Beijing, China, 2018.
10. Yang, L.B.; Ren, X.N.; Ge, C.C.; Yan, Q.Z. Status and development of powder metallurgy nickel-based disk superalloys. *Int. J. Mater. Res.* **2019**, *110*, 901–910. [CrossRef]
11. Zhang, Y.W. Investigation of porosity in superalloy powder. *J. Iron Steel Res.* **2002**, *14*, 73–76.
12. Hu, L.X.; Feng, X.Y. The research and development of powder metallurgy superalloy. *Powd. Metal. Ind.* **2018**, *28*, 1–7.
13. Zhang, G.X.; Han, S.B.; Sun, Z.K. Effects of thermal induced porosity on mechanical properties of PM superalloy. *Powd. Metal. Ind.* **2015**, *25*, 42–45.
14. Zhang, H.; Xiong, J.Y.; Wang, C.; Ma, D.X. Effects of thermal induced porosity on the properties of FGH97 powder metallurgy superalloys. *Fail. Anal. Prev.* **2019**, *14*, 90–95.
15. Miner, R.V.; Dreshfield, R.L. Effects of fine porosity on the fatigue behavior of a powder metallurgy superalloy. *Metall. Trans. A.* **1981**, *12*, 261–267. [CrossRef]

16. Wang, P.X.; Zou, Z.Y. The study of thermal induced porosity (TIP) on FGH95 and Rene′ 95 P/M superalloy. *J. Beijing Univ. Iron Steel Technol.* **1987**, *S1*, 118–123.
17. Stefanescu, D.M. Computer Simulation of Shrinkage Related Defects in Metal Casting—A Review. *Int. J. Cast Metals Res.* **2005**, *18*, 129–143. [CrossRef]
18. Lee, P.D.; Chirazi, A.; See, D. Modeling Microporosity in Aluminum—Silicon Alloys: A review. *J. Light Met.* **2001**, *1*, 15–30. [CrossRef]
19. Lee, P.D.; Hunt, J.D. Hydrogen porosity in directionally solidified aluminum-copper alloys: A mathematical model. *Acta Mater.* **2001**, *49*, 1383–1398. [CrossRef]
20. Carlson, K.D.; Lin, Z.P.; Beckermann, C. Modeling the effect of finite-rate hydrogen diffusion on porosity formation in aluminum alloys. *Metall. Mater. Trans. B* **2007**, *38B*, 541–555. [CrossRef]
21. Monastyrskiy, V.P. Modeling of Porosity Formation in Ni-based Superalloys. In Proceedings of the 8th Pacific Rim International Conference on Modeling of Casting and Solidification Process (MCSP8-2010), Incheon, Republic of Korea, 12–15 April 2010.
22. Bokstein, B.S.; Epishin, A.I.; Link, T.; Esin, V.A.; Rodin, A.O.; Svetlov, I.L. Model for the porosity growth in single-crystal nickel-based superalloys during homogenization. *Scripta Mater.* **2007**, *57*, 801–804. [CrossRef]
23. Torroba, A.J.; Koeser, O.; Calba, L.; Maestro, L.; Carreño-Morelli, E.; Rahimian, M.; Milenkovic, S.; Sabirov, I.; LLorca, J. Investment casting of nozzle guide vanes from nickel-based superalloys: Part 1—Thermal calibration and porosity prediction. *Integr. Mater. Manuf. Innov.* **2014**, *3*, 344–368. [CrossRef]
24. Yang, J.L.; Zhu, X.M.; Tan, J.J.; Xiong, J.Y. Microstructure and properties of argon atomization FGH97 P/M superalloy. *Rare Metal. Mat. Eng.* **2019**, *48*, 4095–4100.
25. *GB/T 15749-2008[S]*; Measuring Method in Quantitative Metallography. General Administration of Quality Supervision, Inspection and Quarantine of the People's Republic of China. Standardization Administration of the People's Republic of China: Beijing China, 2008.
26. Prasad, M.R.G.; Gao, S.W.; Vajragupta, N.; Hartmaier, A. Influence of Trapped Gas on Pore Healing under Hot Isostatic Pressing in Nickel-Base Superalloys. *Crystals* **2020**, *10*, 1147. [CrossRef]
27. Tan, J.J.; Guo, J.Z.; Long, A.P.; Li, Q.T.; Xiao, L. Effects of Different Atomization Method on Powder Property, Microstructure and Low Cycle Fatigue Property of FGH97 Alloy. *IOP Conf. Ser. Mater Sci Eng.* **2020**, *774*, 012067. [CrossRef]
28. Williams, S.T.; Withers, P.J.; Todd, I.; Prangnell, P.B. Porosity regrowth during heat treatment of hot isostatically pressed additively manufactured titanium components. *Scripta Mater.* **2016**, *122*, 72–76. [CrossRef]
29. Zhang, Y.W.; Shangguan, Y.H. Research and development in P/M superalloy. *Powd. Metal. Ind.* **2004**, *14*, 30–43.
30. Strumza, E.; Hayun, S.; Barzilai, S.; Finkelstein, Y.; David, R.B.; Yeheskel, O. In situ detection of thermally induced porosity in additively manufactured and sintered objects. *J. Mater. Sci.* **2019**, *54*, 8665–8674. [CrossRef]
31. Prybylowski, J.; Pelloux, R.M.; Price, P. Effects of argon contamination in PM hot isostatically pressed nickel base superalloy. *Powder Metall.* **1984**, *27*, 107–111. [CrossRef]
32. Murray, N.G.D.; Dunand, D.C. Effect of thermal history on the superplastic expansion of argon-filled pores in titanium: Part I kinetics and microstructure. *Acta Mater.* **2004**, *52*, 2269–2278. [CrossRef]
33. Menasche, D.B.; Shade, P.A.; Lind, J.; Li, S.F.; Bernier, J.V.; Kenesei, P.; Schuren, J.C.; Suter, R.M. Correlation of thermally induced pores with microstructural features using high energy X-rays. *Metall. Mater Trans. A* **2016**, *47A*, 5580–5588. [CrossRef]
34. Liu, M.D.; Zhang, Y.; Huang, H.B.; Li, K.M.; Han, S.B.; Zhao, J.J.; Zhang, Y.W. Analysis of heat treatment cracking of one Ni-based powder metallurgy superalloy disk. *Powd. Metal. Ind.* **2017**, *27*, 48–52.
35. Sellars, C.M.; Whiteman, J.A. Recrystallization and grain growth in hot rolling. *Met. Sci.* **1978**, *13*, 187–194. [CrossRef]
36. Reed, R.C. *The Superalloys Fundamentals and Applications*; Cambridge University Press: New York, NY, USA, 2006.